P2.34 THE EFFECTS OF ENTRAINMENT AND MIXING ON THE DROPLET SIZE DISTRIBUTIONS IN CUMULI

Schlüter Merja Helena[1] *, Steven K. Krueger[1], and Chwen-Wei Su[1]
[1]University of Utah, Salt Lake City, Utah

1. INTRODUCTION

Shallow, maritime, cumulus convection is one of the most prevalent cloud types on the planet. Trade wind cumuli typically extend to no greater than 4 km altitude, the height of the tropical trade wind inversion, and are dominanted by warm rain processes. They are ubiquitous over much of the tropical oceans, and characterizing their properties is important for understanding the hydrological cycle and with that the global energy balance and climate.

At the smallest microphysical scale, the most fundamental problem - recognized for over half a century - is explaining the rapid onset of precipitation in shallow tropical clouds. It is closely related to the population of cloud droplets produced by condensation. The growth process must account for growth from condensation nuclei to raindrops in about 15-20 minutes. The onset of precipitation for example depends on the likelihood of a few big droplets to grow enough for the collection process to become efficient at producing precipitation embryos (Pruppacher and Klett 1997). The short time for the rain development requires the droplet spectra to be broad enough for droplets to have a high rate of collision.

Stommel (1947) was the first to note that cumulus clouds had to be significantly diluted by environmental air from above the cloud base in order to explain their temperature and liquid water content profiles. In most one-dimensional (1D) models of cumulus clouds, it has been assumed that entrainment occurs continuously and that the entrained air is instantaneously mixed across the entire cloud (e.g., Stommel 1947; Manton and Warner 1982.)

Latham and Reed (1977) studied the effects of small scale turbulent entrainment mechanism and introduced the concept of inhomogeneous mixing. Burnet et al. (2006) found from the observational study of RICO (Rain In Cumulus over the Ocean) data that the mixing process is neither homogeneous nor inhomogeneous.

Jensen (1989) suggested that mixing of environmental air with cloudy parcels with high or low entrained fraction values may result in wider droplet spectra.

Krueger et al. (1997) developed the EMPM (Explicit Mixing Parcel Model) to study a series of individual entrainment and mixing events separated by periods of adiabatic ascent. This model explicitly represents spatial variability due to entrainment and turbulent mixing down to the smallest turbulent scales in a 1D domain. Su et al. (1998) included explicit droplet growth and showed that the EMPM results favourable compared with droplet size spectra measured in Hawaiian trade wind cumulus clouds. Several thousand individual droplets evolve by condensation or evaporation according to their local environment. Turbulent mixing is incorporated by the 1D linear eddy model based on Kerstein (1991) using the triplet map and molecular dissipation is resolved.

In this study the EMPM is used to examine how entrainment and mixing affect spectral broadening.

2. NUMERICAL EXPERIMENTAL SETUP

We simulated single entrainment events with the EMPM followed by isobaric mixing after an adiabatic ascent to study the effects of entrainment and mixing on the droplet size distribution (DSD). Broadening the droplet size spectra depends on inhomogeneities in the cloud micro structure produced by entrainment and mixing of subsaturated air.

In all simulations, the domain size was 20 m (x) $\times$ 1 mm (y) $\times$ 1 mm (z) with 12000 grid cells.

To develop different types of entrainment and mixing, the main parameters, which are varied for the simulations, are the environmental relative humidity (RH_e), the entrainment fraction (f), the size of the entrained environmental air filament (d) and the turbulent mixing rate (ϵ). The initial conditions are from the Hawaiian observations of Raga et al. (1990).

The values for the experiment are listed in the Table 1. 2055 droplets initially exist in the domain and are assigned random locations. The updraft velocity is held constant until the entrainment level is reached. Figure 1 shows schematically the model setup and parameters varied.

After an adiabatic ascent, a single entrainment event occurs. After entrainment, the parcel is held at the same pressure level, and mixing occurs until homogenization. The runs were initialized with two different random number seeds to study the sensitivity to the

* *Corresponding author address:* Department of Meteorology, University of Utah, Salt Lake City, UT 84112. E-mail: helena@met.utah.edu

Table 1: Parameters for EMPM with explicit microphysics

parameter	value
cloud base conditions:	
N_d	102.75 cm^3
p_b	963.95 hPa
T_b	293.56 K
q_{vb}	15.73 g kg^{-1}
w	2 m s^{-1}
D	20 m
entrainment parameters:	
d	1, 2 (control), 6, 10 m
f	0.1 - 0.9
RH_e	0.874 (control), 0.437, 0.219
ϵ	10^{-2} (control), 5×10^{-3}, 10^{-4}, 10^{-6}, ∞ m^{2}s^{-3}

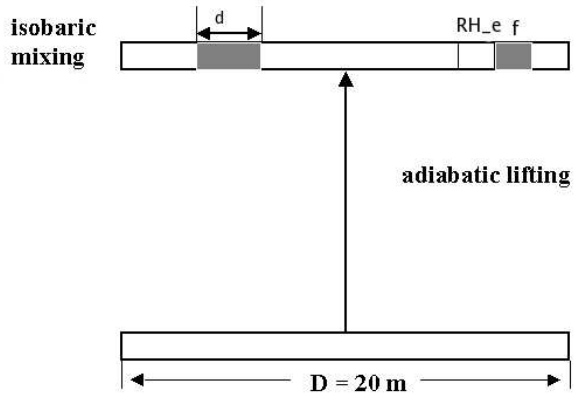

Figure 1: Schematic diagram of the model setup.

random numbers. The EMPM results include the histories of the droplet radii and the locations in the domain and the corresponding histories of temperature and mixing ratio.

3. SIMULATION RESULTS

3.1. Single entrainment events

Figure 2 shows the droplet size distribution (DSD) after mixing is completed for $f = 0.3$ for reduced environmental humidity cases compared to the control case for two realizations and instant mixing case (one realization). The droplets are categorized by radius with a bin of Δr = 0.1 μm if not mentinoned otherwise. The largest spectral width is obtained with the driest air entrained. The peak of the DSD with the dri-

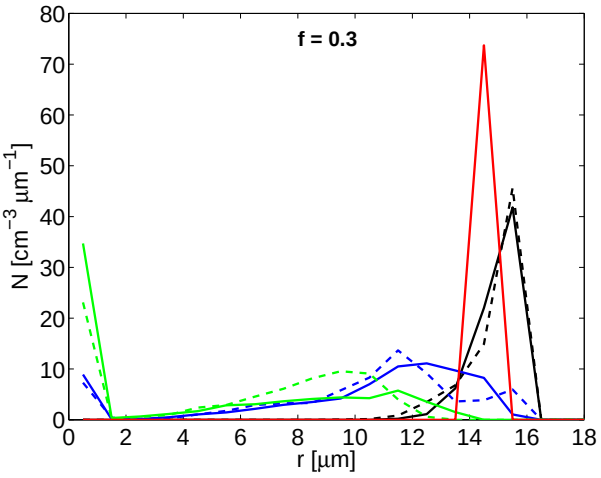

Figure 2: Droplet spectra for $RH_e = 0.874$ (black) and instant mixing (red), 0.437 (blue) and 0.219 (green), for entrained fraction $f = 0.3$.

est entrained air is decreased most and shifted towards smaller radius sizes. Drier entrained air requires more evaporation and complete evaporation of some droplets to regain saturation and therefore the size distribution is broadened towards smaller sizes. Why are there such big differences among the DSDs in Figure 2? The only way is that the DSD depends on the mixing process which is characterized by the mixing and evaporation timescales.

Instant mixing assumes inhomogeneities are gone instantly. The outcoming DSD for that is shown in Figure 2 (red). The statistical properties of the droplet spectrum may depend upon the length of time the inhomogeneities in the local saturation fields persist. The timescale for homogenization of an entrained blob of size d through the process of turbulent mixing is:

$$\tau_m = \left(\frac{d^2}{\epsilon}\right)^{\frac{1}{3}}. \qquad (1)$$

The timescale for droplet evaporation (τ_e) depends on the droplet radius and can be estimated from the droplet growth equation:

$$\tau_e \approx -\left(\frac{D^2}{C(p,T)(S-1)}\right), \qquad (2)$$

where D is the diameter of the droplet, S-1 is the supersaturation and C is a function of pressure and temperature.

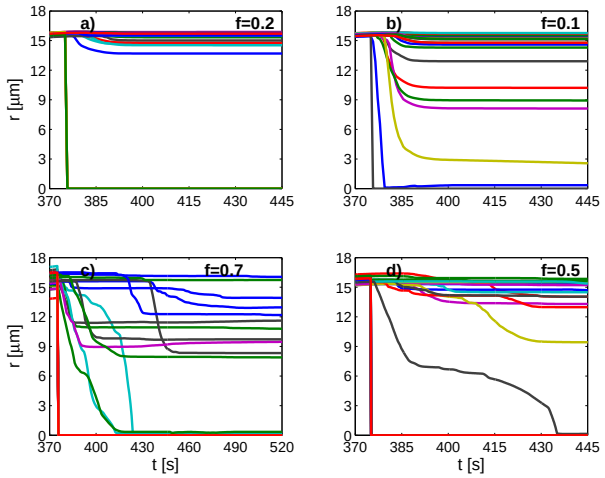

Figure 3: 30 droplet radius histories for the control case (a), $RH_e = 0.291$ (b), $d = 10$ m (c) and $\epsilon = 10^{-6}$ m^{2}s^{-3} (d).

Figure 3 shows the radius histories of 30 droplets for the control, $RH_e = 0.291$, $d = 10$ m and $\epsilon = 10^{-6}$ m^{2}s^{-3} cases from just before entrainment until mixing is completed. It shows that the radius variations with time decrease at different rates for the different cases. For the larger entrained blob and slower mixing cases the reduction in the radius has multiple steps.

Figure 4 shows the DSD for different dissipation rates for $f = 0.7$. The spectrum broadens to larger and smaller droplet radii and lower concentration peaks for the two slowest mixing cases. Note that for the slowest mixing case the droplet radii squared are almost uniformly distributed over all radius size categories. The

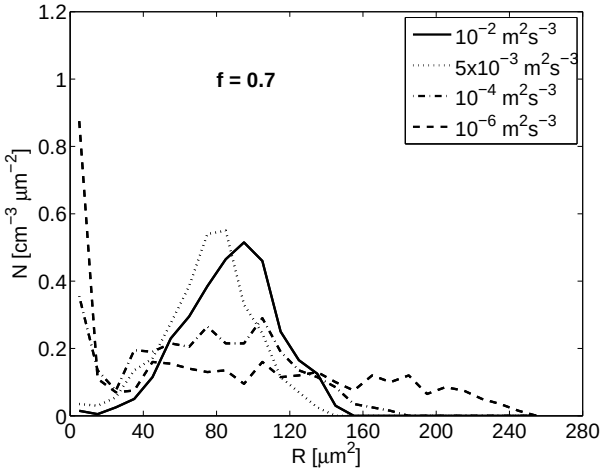

Figure 4: R $\equiv$ r^2 for various dissipation rates for $f = 0.7$.

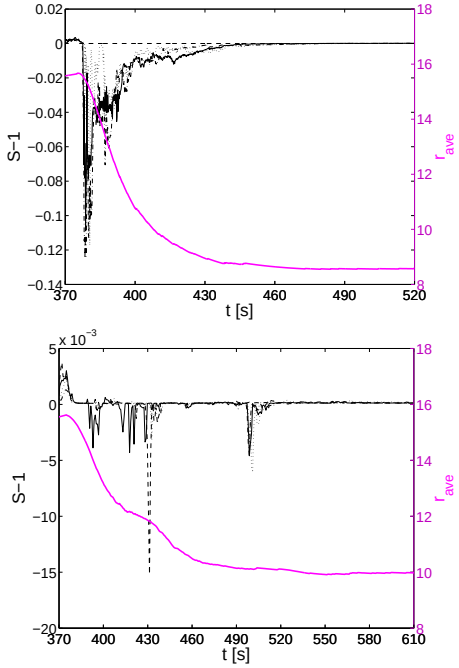

Figure 5: r_{ave} for all r > 0.1 μm and S-1 history of four droplets for $\epsilon = 10^{-4}$ m^{2}s^{-3} (top) and $\epsilon = 10^{-6}$ m^{2}s^{-3} (bottom) for $f = 0.7$.

reason for the difference is evident in Figure 5, which shows the averaged radius (r_{ave}) for all radii > 0.1 and the supersaturation histories for four droplets for $\epsilon = 10^{-4}$ m^{2}s^{-3} (top) and $\epsilon = 10^{-6}$ m^{2}s^{-3} (bottom). The droplets encounter regions of subsaturated air at later times for $\epsilon = 10^{-6}$ m^{2}s^{-3} and the mixing takes longer. Thus, droplets grow or evaporate according to their different local environments, where they stay for a longer time for slower mixing.

Figure 6 shows the DSDs for the different entrained blob sizes ($d = 1$, 2, 10 m) for $f = 0.5$. Note that the dissipation rate for one of the larger entrained blob case ($d = 10$ m), $\epsilon = 10^{-4}$ m^{2}s^{-3}, is lower than the control case. The spectrum for a smaller entrained blob size (blue line) is narrower compared to the control case due to the rapid break down of the smaller entrained eddies. One entrained big blob takes longer to break down. This case is similar to the slow mixing case in Figure 4. The broadening is generally towards smaller radius sizes, except with also slower mixing the spectral shape shows braodening features towards larger sizes.

To examine how the droplet spectra depend on the degree of dilution with the entrained air, we show the droplet spectral width versus the entrainment fraction for the various cases. The droplet spectral width (σ_r) is the standard deviation of the distribution of the droplet radii.

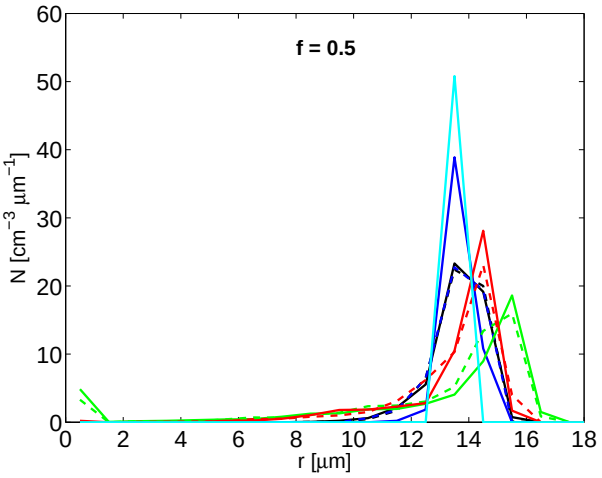

Figure 6: DSDs for various entrained blob sizes: 1. m (blue), 2. m (black (control), light blue (instant mixing)), 10. m (red) for $\epsilon = 10^{-2}$ m^{2}s^{-3} and 10. m (green) for $\epsilon = 10^{-4}$ m^{2}s^{-3}, for $f = 0.5$ and $RH_e = 0.874$.

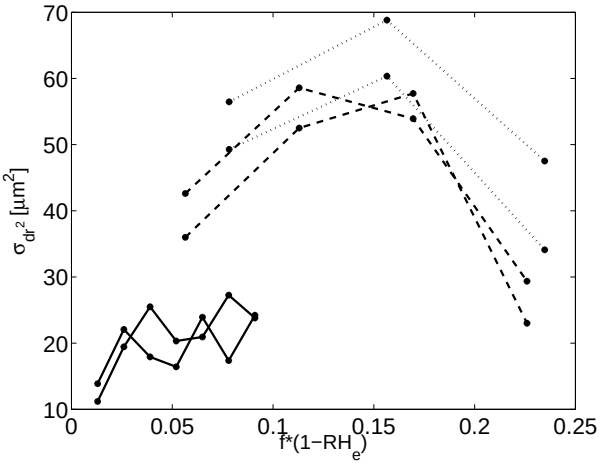

Figure 7: σ_{dr^2} of $RH_e = 0.87$ (solid), $RH_e = 0.44$ (dashed) and $RH_e = 0.22$ versus $f(1 - RH_e)$.

Figure 7 shows the calculated droplet spectral width (σ_{dr^2}) of Δr^2 before entrainment and after isobaric mixing is completed for two realizations for the control case $RH_e = 0.874$ (solid lines), 0.437 (dashed lines) and 0.219 (dotted lines) as a function of $f(1 - RH_e)$. For the control case there is not much variability of the subsaturation history during mixing. σ_{dr^2} is much larger for both drier entrained air cases because there is more variability in the subsaturation history. At a degree of dryness greater than 0.15 both drier entrained air cases have decreased widths. The reason is that all droplets evaporate, partially or totally. σ_r for different dissipation rates compared to the control case is

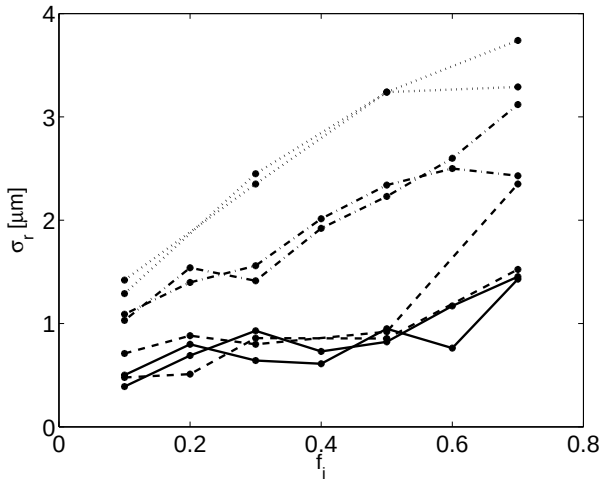

Figure 8: σ_r for different dissipation rates: $\epsilon = 10^{-2}$ m^{2}s^{-3} (solid), $\epsilon = 5 \times 10^{-3}$ m^{2}s^{-3} (dashed), $\epsilon = 10^{-4}$ m^{2}s^{-3} (dashed dotted) and $\epsilon = 10^{-6}$ m^{2}s^{-3} (dotted) versus different entrained air fractions f_i.

shown as a function of f_i in Figure 8. It shows that high turbulence leads to lower σ_r, low turbulence levels give significantly wider droplet spectra, which increases linearly with increased entrainment fractions.

Figure 9 shows the calculated droplet spectrum width as a function of entrained air fraction for different blob sizes. Larger or smaller entrained blob sizes with $\epsilon = 10^{-2}$ m^{2}s^{-3} up to an entrained fraction of 0.3 do not contribute much to an increase in the spectral width. For $d = 10$ m the case with $\epsilon = 10^{-4}$ m^{2}s^{-3} has wider spectra.

The characteristics of the droplet spectra depend on the ratio of the mixing and evaporation timescales:

$$\gamma = \frac{\tau_m}{\tau_e}. \tag{3}$$

The ratio determines which effect is faster, which influences the shape of the DSD after mixing is completed. If $\tau_m \ll \tau_e$, the entrained air is immediately mixed across the cloud segment, and the droplets evaporate into the uniform air mixture. If $\tau_m \gg \tau_e$, the mixing is inhomogeneous and droplets evaporate locally due to their subsaturated environments, while in other areas the droplets are unaffected and do not evaporate. Table 2 shows the mixing and evaporation timescales and their ratios with respect to the various cases. The different cases conducted show a variety of different ratios. Comparing these to their DSDs, one can classify the cases. If $\gamma \geq 1$ the mixing timescale is similar or greater than the evaporation timescale and the DSD is widest for all f-values. This holds for the $RH_e =$

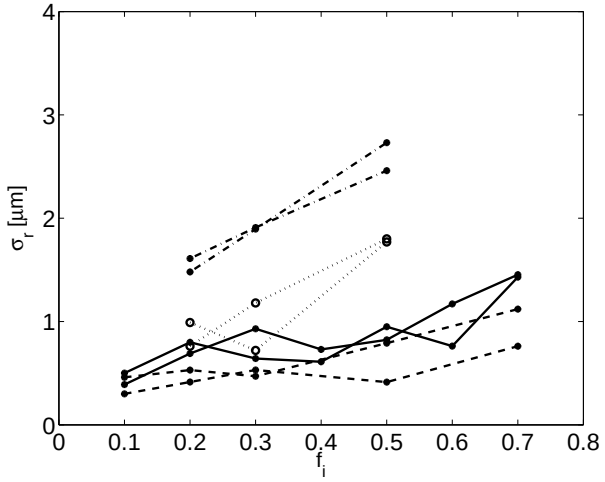

Figure 9: σ_r for different different blob sizes d = 1 m (dashed), d =2 m (solid), and larger ds with $\epsilon = 10^{-2}$ m^{2}s^{-3} (dotted) and $\epsilon = 10^{-4}$ m^{2}s^{-3} (dashed dotted) versus f_i.

Table 2: Timescales τ_e and τ_m and their ratio for the various cases.

cases	$\tau_m[s]$	$\tau_e[s]$	γ
control	7.3	19.	0.3
d = [m]:			
1	4.6	19.	0.2
4	12.	19.	0.6
6	15.	19.	0.8
10	22.	19.	1.1
10 for $\epsilon = 10^{-4}$	100.	19.	5.2
$\epsilon = [m^2 s^{-3}]$:			
5×10^{-3}	9.3	19.	0.5
10^{-4}	34.	19.	1.8
10^{-6}	160.	19.	8.2
RH_e :			
0.44	7.4	4.4	1.7
0.22	7.4	3.1	2.4

0.437 and 0.219, d = 10 m and slower mixing cases. If $1 \geq \gamma \geq 0.1$ the DSD is not much broadened: see the control, smaller blob size, $\epsilon = 5 \times 10^{-3}$ m^{2}s^{-3} and d = 4 and 6 m cases.

To analyze the data microphysically, the experiments can be examined with the N - V diagram as by Gerber et al. (2001) and Burnet and Brenguier (2006) in cumulus (Cu), see Figure 10. N is the droplet concentration and V is the mean volume of the droplets. Both values are normalized by their adiabatic values before entrainment. The product of the coordinates is proportional to the normalized LWC, which is represented by red dashed lines of LWC dilution ratio. The environmental relative humdity lines were generated with the linear mixing concept followed by saturation adjustment, which represents the homogeneous mixing process. That is, for each entrained fraction the cloud is diluted by that fraction and homogenized, so all droplets evaporate a bit.

It still is not clear whether the reduction of the liquid water ratio by entrainment is accounted for by a dilution of the number concentration of droplets or a reduction of the droplet size, or both (Burnet and Brenguier 2006).

Figure 10 shows N versus V for the instant mixing and reduced RH_e cases. The green squares of the instant mixing case for entrained fractions f = 0.1, 0.3, 0.5 and 0.7 lay exactly on the 0.874 environmental relative humidity line. In this case, the droplet number concentration is diluted proportionally to the amount of entrained air. The liquid water mixing ratio deficit is accounted for by droplet evaporation and a decrease of the droplet size.

The red circles represent the case with RH_e = 0.437 for fractions f = 0.1 - 0.4. N is even more reduced due to droplets that completely evaporate. The values do not follow any specific mixing behavior after f = 0.2.

The yellow diamonds represent the case with RH_e = 0.219 for f = 0.1 - 0.3. These values depart most from the corresponding relative humidity line.

4. CONCLUSIONS

This study has examined the evolution of droplet spectra after entrainment for isobaric mixing for different parameters such as different entrained blob sizes, the entrainment fraction, the environmental relative humidity and different dissipation rates. The spectral width is different for different parameters depending on the timescales for mixing and evaporation and the entrainment fraction.

Reducing the moisture in the entrained air or increasing the entrained blob size broadens the spectrum at smaller radius sizes, whereas lower dissipation rates enhances broadening of the spectrum at both extremes of the radius sizes.

The N - V analysis shows evidence of total evaporation of some droplets for DSDs with large spectral widths.

The analysis of the timescales shows that broadening of the DSD is favored by relatively long mixing and short evaporation timescales. The droplet spectral width is widest for cases with reduced environmental

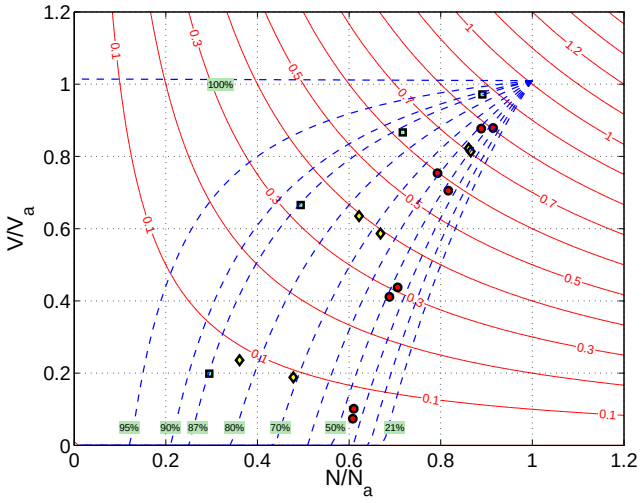

Figure 10: N and V ratios for the $RH_e = 0.437$ (red circles) and 0.219 (yellow diamonds) and instant mixing (green squares) case with $RH_e = 0.874$.

relative humidity, reduced dissipation rate, or bigger blob sizes.

Our results suggest that it is possible to parameterize the impact of entrainment and mixing on the DSD in this simple scenario as a function of the two time scales and the volume fraction of the entrained air.

The analysis has led to some clarification of the mixing process involved in the evolution of droplet spectra.

It is not feasible up to now with airborne microphysical measurements to isolate single entrainment and mixing events, nor to follow their impact on droplet spectra. The EMPM has proved itself to be a useful tool for that because it can track the evolving spatial structure and follows the histories of individual droplets. It provides information at resolutions which are comparable to aircraft measurements in field experiments measuring real clouds. This study generated new questions and gave insights on how to proceed in future studies.

ACKNOWLEDGMENTS. This research was supported by the National Science Foundation (NSF) under Grant No. ATM-0346854.

References

Burnet, F., and J.-L. Brenguier, 2006: Experimental study of the entrainment-mixing process. *J. Atmos. Sci.,* submitted.

Gerber, H., J. Jensen, A. Davis, A. Marshak, and W. Wiscombe, 2001: Spectral density of cloud liquid water content at high frequencies. *J. Atmos. Sci.*, **58**, 497–503.

Jensen, J., and M. Baker, 1989: A simple model of droplet spectral evolution during turbulent mixing. *J. Atmos. Sci.*, **46**, 2812–2829.

Kerstein, A. R., 1991: Linear-eddy modeling of turbulent transport. part 6, microstructure of diffuse scalar mixing fields. *Combust. Sci. and Tech.*, **231**, 361–394.

Krueger, S., C.-W. Su, and P. McMurtry, 1997: Modeling entrainment and finescale mixing in cumulus clouds. *J. Atmos. Sci.*, **54**, 2697–2712.

Latham, J., and R. Reed, 1977: Laboratory studies of the effects of mixing on the evoluiton of cloud droplet spectra. *Quart. J. Roy. Meteor. Soc.*, **103**, 297–306.

Manton, M. J., and J. Warner, 1982: On the droplet distribution near the base of cumulus clouds. *Quart. J. Roy. Meteor. Soc.*, **108**, 917–928.

Pruppacher, H., and J. Klett, 1997: *Microphysics of Clouds and Precipitation*. Kluwer Academic Publishers.

Raga, G., J. B. Jensen, and M. B. Baker, 1990: Characteristics of cumulus band clouds of the coast of hawaii. *J. Atmos. Sci.*, **47**, 2708.

Stommel, H., 1947: Entrainment of air into a cumulus cloud. *J. Atmos. Sci.*, **4**, 91–94.

Su, C.-W., S. K. Krueger, P. A. McMurtry, and P. H. Austin, 1998: Linear eddy modeling of droplet spectral evolution during entrainment and mixing in cumulus clouds. *Atmos. Res.*, **47–48**, 41–58.